Study of TOF methods used for identifying thermal neutron, fast neutron and gamma in the scintillator

Y.K. Sun[a,b,*], X.K. Zhao[a,b], H. Zhang[a,b], M. Shao[a,b], Z.B. Tang[a,b], C. Li[a,b], H.F. Chen[a,b]

[a] *Department of Modern Physics, University of Science and Technology of China, Hefei 230026, China*

[b] *State Key Laboratory of Particle Detection and Electronics (USTC-IHEP), China*

Abstract

Neutron fluxes are often contaminated with gamma, to which the detectors are sensitive. Pulse shape analysis (PSD) is frequently used to identify neutron and gamma. However, it is difficult to distinguish fast neutron and thermal neutron. At the same time, time of flight is up to microsecond, TOF method can not be applied to identify thermal neutron. An experiment with an AmBe neutron source was set up and provided data. From gained pulse information, time spectrum of flight neutrons can be extracted. Neutron energy spectrum can be gained by measuring time of flight neutrons. We combine TOF and pulse shape analysis to separate neutrons and gammas in a mixed emission field with the boron-loaded plastic scintillator.

Keywords: TOF, Fast neutron, Thermal neutron, Gamma, identification

1. Introduction

The China Accelerator Driven subcritical System (C-ADS) project aim to solve the nuclear waste problem and the resource for nuclear power plants in China. ADS is a subcritical reactor driven by the spallation neutrons, which are produced by high-energy protons directed at a high-atomic number target. It is important and significant to design a new detector for identifying neutron and gamma.

*Email address: sunming@mail.ustc.edu.cn

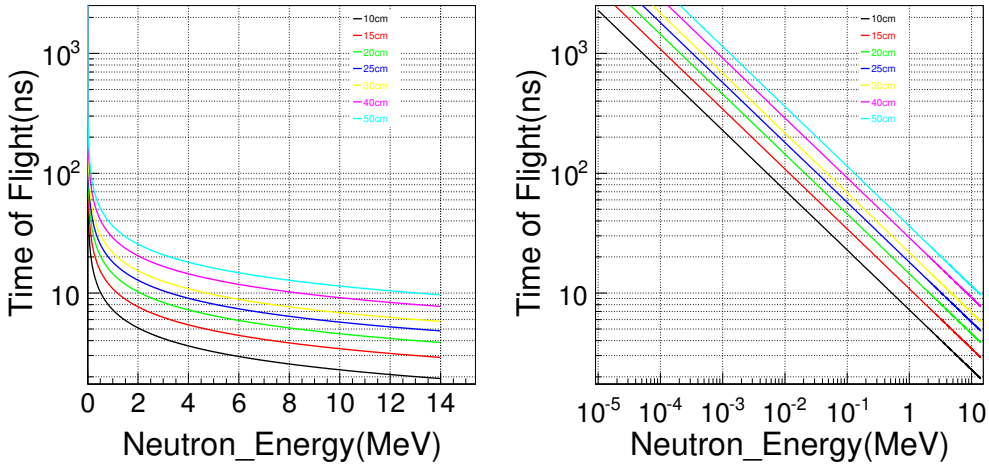

Figure 1: Time of flight as function of neutron's Energy. (Upper) Fast Neutron. (Lower) Thermal neutron.

Time of flight method can be used to identify fast neutron and γ. Figure 1 shows the time of flight from neutron with different energy. From the figure 1(b), we can see that the time of thermal neutron's flight is up to some microsecond. Because of low velocity, it is difficult to identify thermal neutron.

Liquid scintillator solutions are widely used for fast neutron spectroscopy and n/γ discrimination, thermal neutrons can be detected with boron loaded liquid scintillator EJ-399 A [2]. However, flammability and potential for leaks are distinct disadvantages of organic liquids [3].

The sensitivity of boron-loaded plastic scintillator to thermal neutrons is achieved by using the capture reaction on a nucleus of ^{10}B, according to Ref [1]:

$$^{10}B + n = \begin{cases} ^{7}Li + ^{4}He, Q = 2.792MeV, 6\% \\ ^{7}Li + ^{4}He + \gamma(480keV), Q = 2.310MeV, 94\% \end{cases}$$

^{10}B has high cross-sections for thermal neutron and high natural abundance (19.8%). Charged reaction products, ^{7}Li and ^{4}He require only several micrometers to be stopped in the scintillator. ^{7}Li and ^{4}He products also

have significantly different stopping power, dE/dx, from minimum ionizing particles such as recoiled electrons(γ-rays).

The probability of emitting γ, whose feature energy is 480 keV, is around 96 % in the capture reaction. If plastic scintillator is sensitive to γ(480 keV) from the capture reaction on a nucleus of ^{10}B, we can identify thermal neutron by γ energy spectrum.

Neutrons are produced by $^{241}_{95}Am/Be$ source. Equation 1 represents the nuclear reaction and the energy level scheme of ^{12}C is in the Figure 2.

$$^{9}Be + {}^{4}\alpha \rightarrow {}^{12}C + n + \gamma(4.44MeV) + 5.7MeV \quad (1)$$

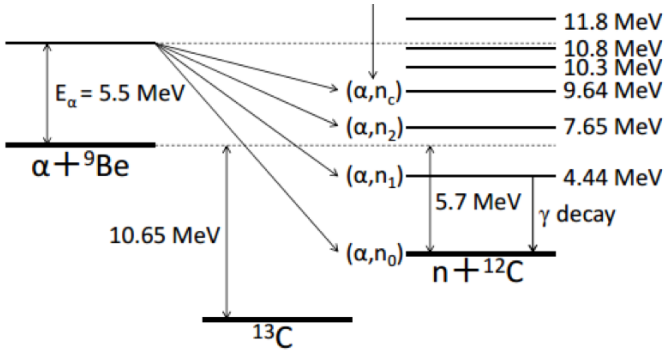

Figure 2: Energy level scheme of ^{12}C .

2. Experimental simulation and measurement

2.1. Experimental System

The neutron detector consists of EJ-254, EJ-200 and four same type PMT(Photomultiplier tubes, R2083,H2431-50, Hamamatsu). Figure 3 (a) displays the size of Photomultiplier tubes, Fig. 3 (c) shows the detail of plastic scintillator detector.

This plastic scintillator(EJ-254) [4] contains natural boron at concentrations up to 1% by weight. Practical boron concentrations down to 0.2% are available. EJ-200 [5] does not contain natural boron and combines the two important properties of long optical attenuation length and fast timing which make it particularly useful for time-of-flight systems using scintillators

greater than one meter long. The size of EJ-254 is 4 cm × 4 cm × 20 cm, another is 4 cm × 4 cm × 50 cm. In order to attenuate $\gamma - rays$ and moderate neutrons, Pb (5 cm) and high density polyethylene (6 cm) were placed between the scintillator and the source.

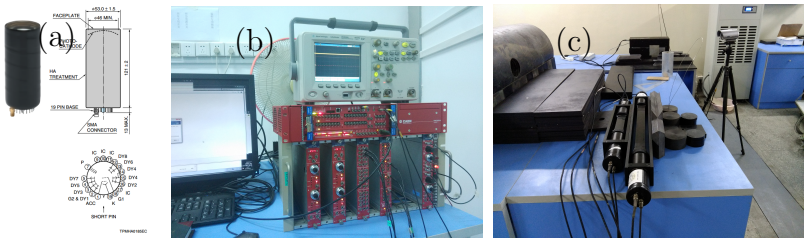

Figure 3: Experimental instruments: (a) PMT(Photomultiplier tubes, R2083,H2431-50, Hamamatsu). (b) Data Acquisition(DAQ). (c) Plastic scintillator detector.

Neutrons are produced by $^{241}_{95}Am/Be$ source. $^{241}_{95}AmBe$ has a half-life of 432.7 years. The decay is branched into 6E-5 neutron and 4E-5 γ(4.43 MeV) per Am decay [9]. At the same time, ^{22}Na and ^{241}Am is used to calibrate particle energy [9].

DAQ system is shown in the figure 3 (b), which includes VME crate (VME8004A), VME master module(V1718), flash ADC(V1729A), discriminator(N840), fold logic unit(N405) and power(N471).

As a contrast, we have performed two group experiments as listed in the figure 4. The distance of two plastic scintillators arranged in parallel is 40 cm. The center of plastic scintillator is against to each other. Figure 4 (a) shows neutron source is close to EJ254, Fig. 4 (b) shows that close to EJ200.

2.2. Experimental simulation

Monte Carlo simulations with GEANT4 provide a good chance to investigate Time Of Flight and energy spectrum of gamma and neutron. The detector geometry is described in the Fig. 5. We use $QGSP\_BIC\_HP$ of high precision neutron data package as the physics list in the Geant4 simulation.

In the simulation of experimental setup 2, the energy of gamma is set to be 4.43 MeV. The TOF distribution is shown in the figure 6 (a). One is backscattering peak, another produced incident gamma. Figure 6 (b) shows

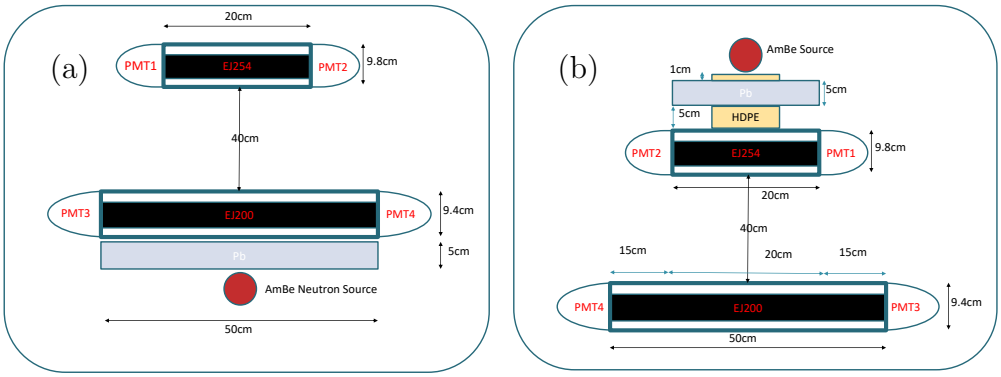

Figure 4: (a) Experimental setup(1): Neutron source be closed to plastic scintillator(EJ200). (b) Experimental setup(2): Neutron source be closed to plastic scintillator(EJ254).

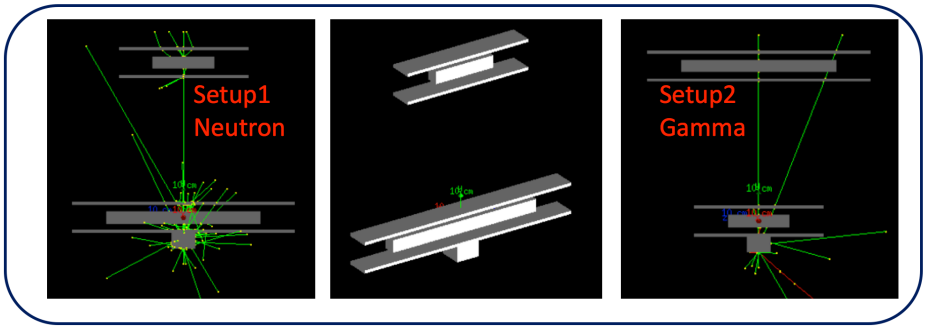

Figure 5: Detector geometry for experimental setup.

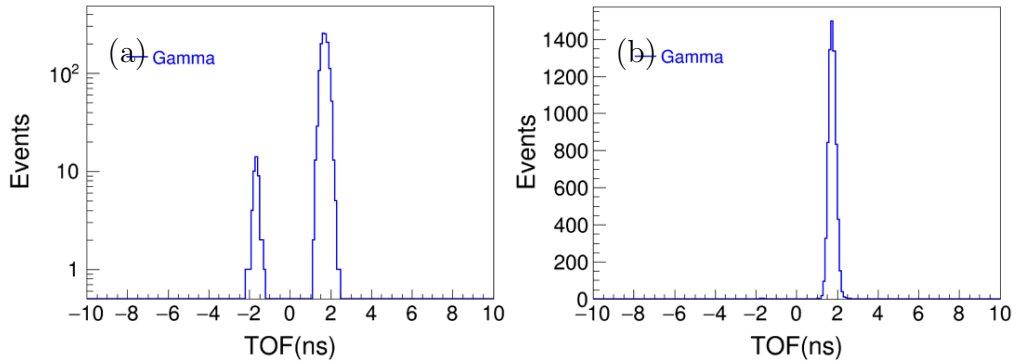

Figure 6: Time of flight of gamma from experimental setup2. (a) TOF distribution of E_γ = 4.43 MeV. (b) TOF distribution of secondary gamma from thermal neutron capture reaction on ^{10}B, E_n = 0.0253 eV.

the TOF distribution of secondary gamma from thermal neutron (0.0253 eV) capture reaction on ^{10}B.

Figure 7 display deposited energy in the plastic scintillators. There is compton edge in the EJ200 plastic scintillator. Due to thermal neutron capture reaction on ^{10}B in the EJ254, energy distribution include compton edge and the full energy peak.

From the results of thermal neutron capture reaction in the Geant4 simulation, characteristic gamma is very useful to identify thermal neutrons with TOF method.

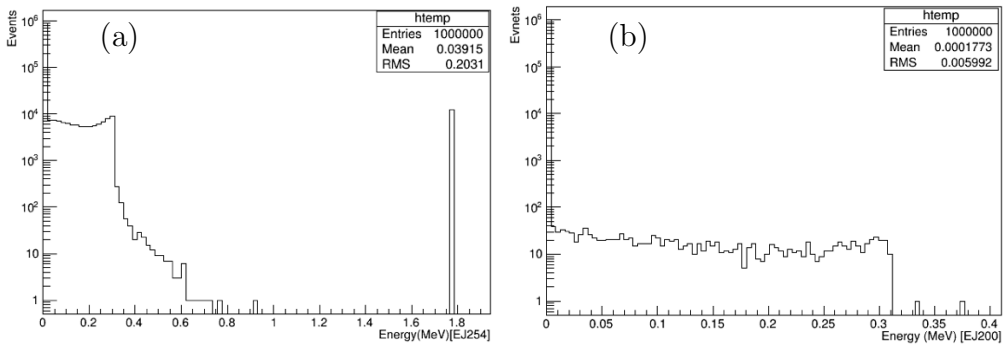

Figure 7: Deposited Energy of thermal neutron from experimental setup2. (a) From plastic scintillator, EJ254. (b) From plastic scintillator, EJ200.

2.3. Experimental measurement

Data sets are consists of pulse wave shapes, which is collected by flash ADC(V1729A). Data flow is shown in Fig. 8. Due to different gain factor for four PMT, different High voltage values are set. Signal from PMT connect with four channels of flash ADC, which trigger is used by inner trigger mode. When flash ADC detect all signals, it will record pulse waves from four PMT.

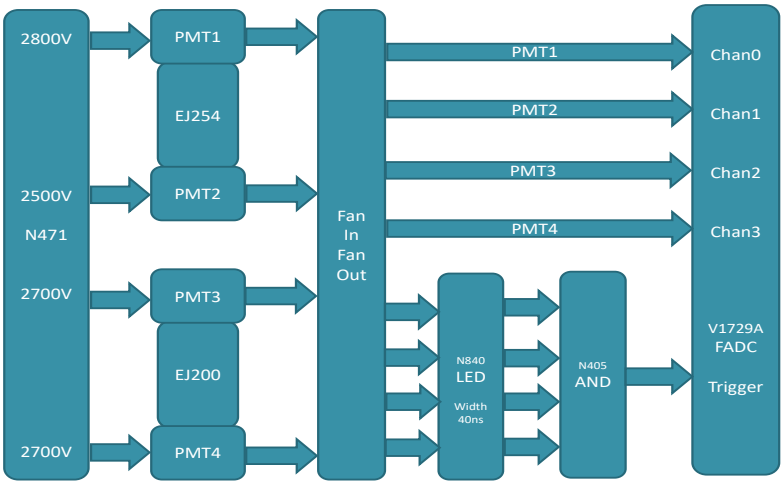

Figure 8: Connection of experimental instruments and data flow .

3. Analysis of experimental data

3.1. Time of Flight

AmBe neutron source of experimental setup 1 is close to EJ200 plastic scintillator , which coupled to PMT3 and PMT4. For experimental setup (2), *AmBe* neutron source is close to EJ254 , which coupled to PMT1 and PMT2. The time of PMT12 is defined as $(T_{PMT1}+T_{PMT2})/2$ and the time of PMT34 is defined as $(T_{PMT3}+T_{PMT4})/2$. After using the definition of time, the length of plastic scintillator has no effect on the time of hitting detector. According to the distance between EJ200 and EJ254, the time of flight of gamma is estimated to be 1.65 ns.

Figure 9 shows the distributions of TOF, which are defined as the time difference between PMT12 and PMT34. After comparing the TOF distributions of two methods, which are from experiment setup (1) and (2), except

relative height of peeks, there is no significant difference between them. We can see that there are two peeks around 2.0 nanosecond. Although all of them are from the time of flight of gamma, the flight paths are very different. First peaks are scattering gamma from back scintillator. Because of different geometric acceptance of plastic scintillators, the peek of setup 2 is smaller than that of setup 1.

Lead (5 cm) can not shield all of gamma from AmBe neutron source, and gamma will pass through two plastic scintillators to produce the second peak. Signal events that TOF is large than 10 ns are from fast neutrons.

From the TOF distribution of setup 2, second peak is higher than experimental setup 1. According to the result of simulation, the signal events not only include gamma from ^{241}AmBe neutron source, but also characteristic gamma (480 keV) from thermal neutron capture reaction on ^{10}B.

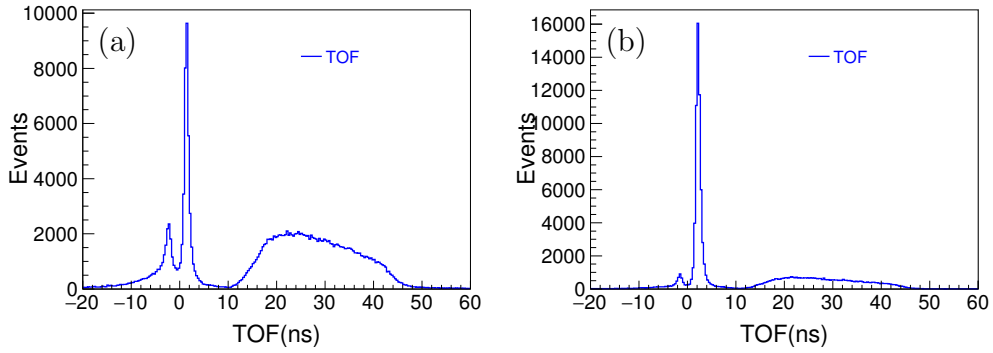

Figure 9: (a) Time of flight from the experiment setup1. (b) Time of flight from the experiment setup2.

3.2. Energy spectrum

To obtain the energy distribution of particles, we can calculate the integration of pulse waves. Integral range is from 20 samples before the maximum peak to 150 samples after the maximum peak.

Figure 10 show the energy spectrum of experimental setup 1. Distributions of Figure 10 (a) and (b) are from the deposited energy of gamma, which is produced by $^{241}AmBe(\alpha, n)$ neutron source. Fast neutrons recoil protons to generate Figure 10 (c) and (d). Figure 10 (e) and (f) are combined the gamma with neutrons. Thermal neutrons also react on B10, and emit feature gamma (480 keV). Then the feature gamma scatter back scintillator and

PMT3 and PMT4 will output pulse signal. The scintillator contained B10 will record the signal of thermal neutron reaction.

Figure 11 show the energy spectrum of experimental setup 2. Distributions of Figure 11 (a) are from the deposited energy of gamma, Li7 and He4, which are produced by $^{241}AmBe(\alpha, n)$ neutron source and production of thermal neutron and B10. Figure 11 (b) The feature gamma (480 keV) produce a compton platform in back scintillator. Fast neutrons recoil protons to generate Figure 11 (c) and (d). Because EJ254 has smaller geometric acceptance than EJ200, there is also a small peak by scattering particles. Figure 11 (e) and (f) are combined the gamma with neutrons.

3.3. Charge correlation

There are two signal output in every scintillator coupling two PMT.

Figure 12 shows the charge correlation distribution of the detector from experimental setup (2). The difference between EJ254 and EJ200 is significant. There are two peeks in the charge correlation distribution of PMT1 and PMT2, which is shown in Figure 12 (a). However, charge correlation distribution of PMT3 and PMT4 is smooth. When the TOF is required to the region: [-20, 10] ns, the distribution in Figure 12 (c) is produced by γ and charged particles, which is from $AmBe$ and thermal neutron reaction. Figure 12 (d)is only from γ. Although the energy of γ from thermal neutron reaction is 480 keV, it is not identified in the charge correlation distribution of PMT3 and PMT4. After TOF is set to be [10, 60] ns, the charge correlation distribution is from fast neutrons, which are shown in Figure 12 (e) and (f).

From the results of the charge correlation distribution, this method of setting experimental setup (2) not only can be used to identify γ and fast neutrons, but also thermal neutrons.

3.4. Signal extraction of thermal neutron

Although we do not distinguish gamma and thermal neutron in the TOF distribution, there is significant difference in the energy spectrum. The number of thermal neutron capture reaction is obtained by fitting the energy distribution. The unbinned maximum likelihood method is performed. The fitting probability density function is described with the sum of Gaussian function and background contribution(signal shape from energy distribution of figure 10 (a).

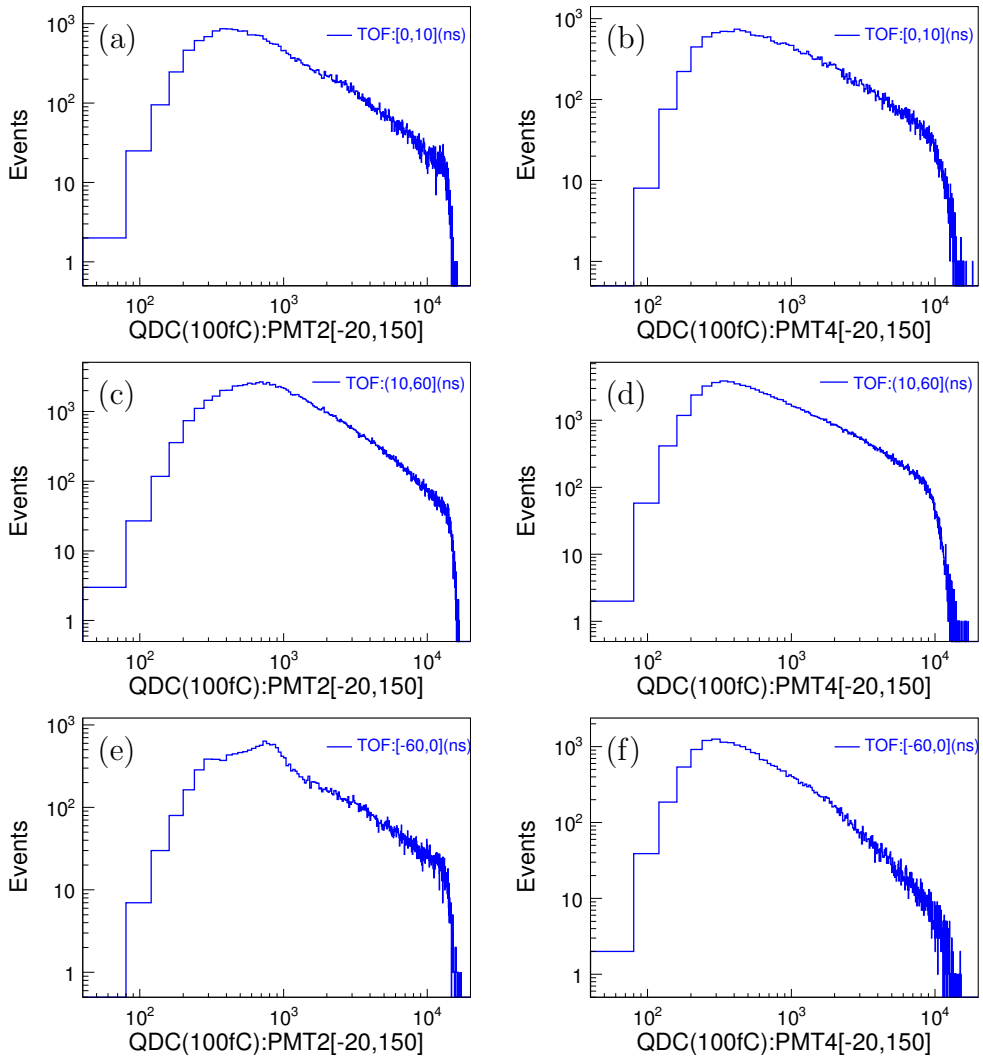

Figure 10: QDC distribution within different TOF region from experiment setup1. (a) and (b) TOF region: [-20, 10]. (c) and (d) TOF region: [10, 60]. (e) and (f) TOF region:[-60, 0].

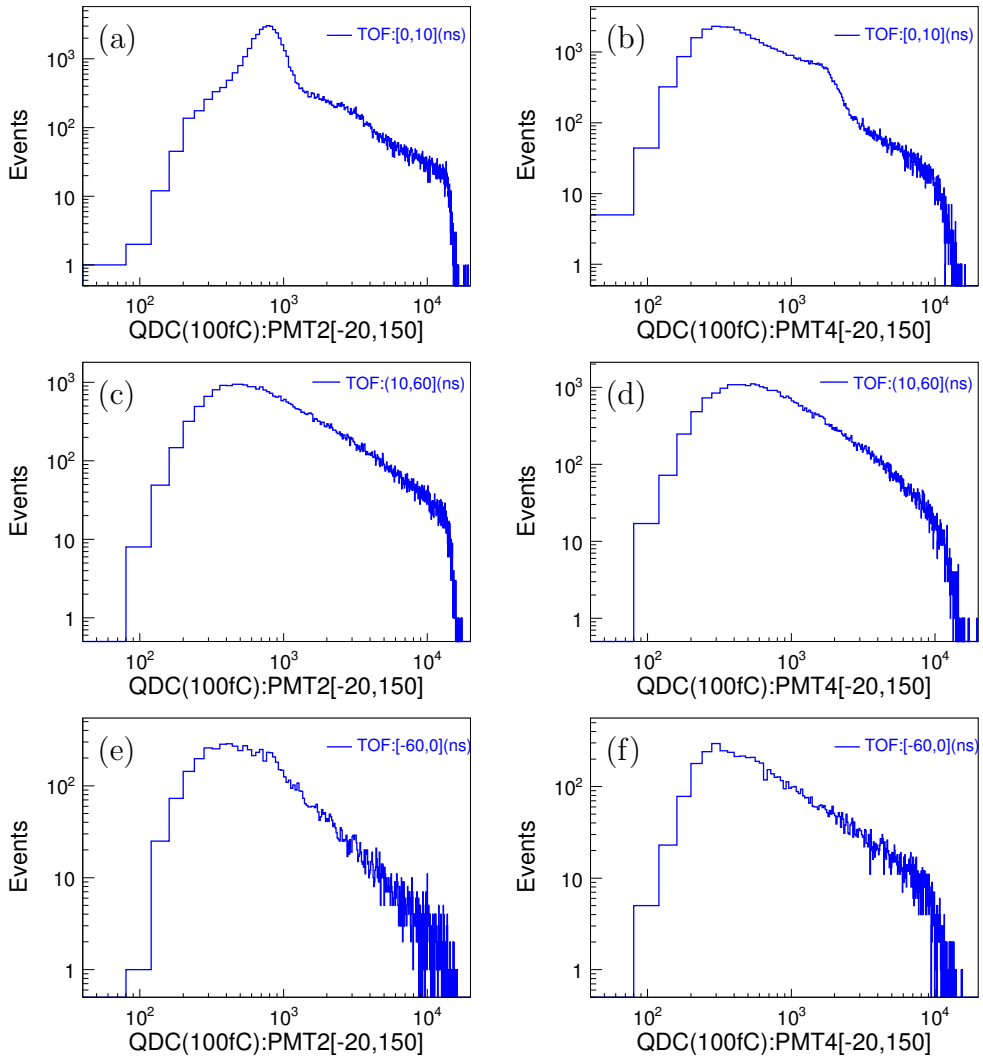

Figure 11: QDC distribution within different TOF region from experiment setup2. (a) and (b) TOF region: [-20, 10]. (c) and (d) TOF region: [10, 60]. (e) and (f) TOF region:[-60, 0].

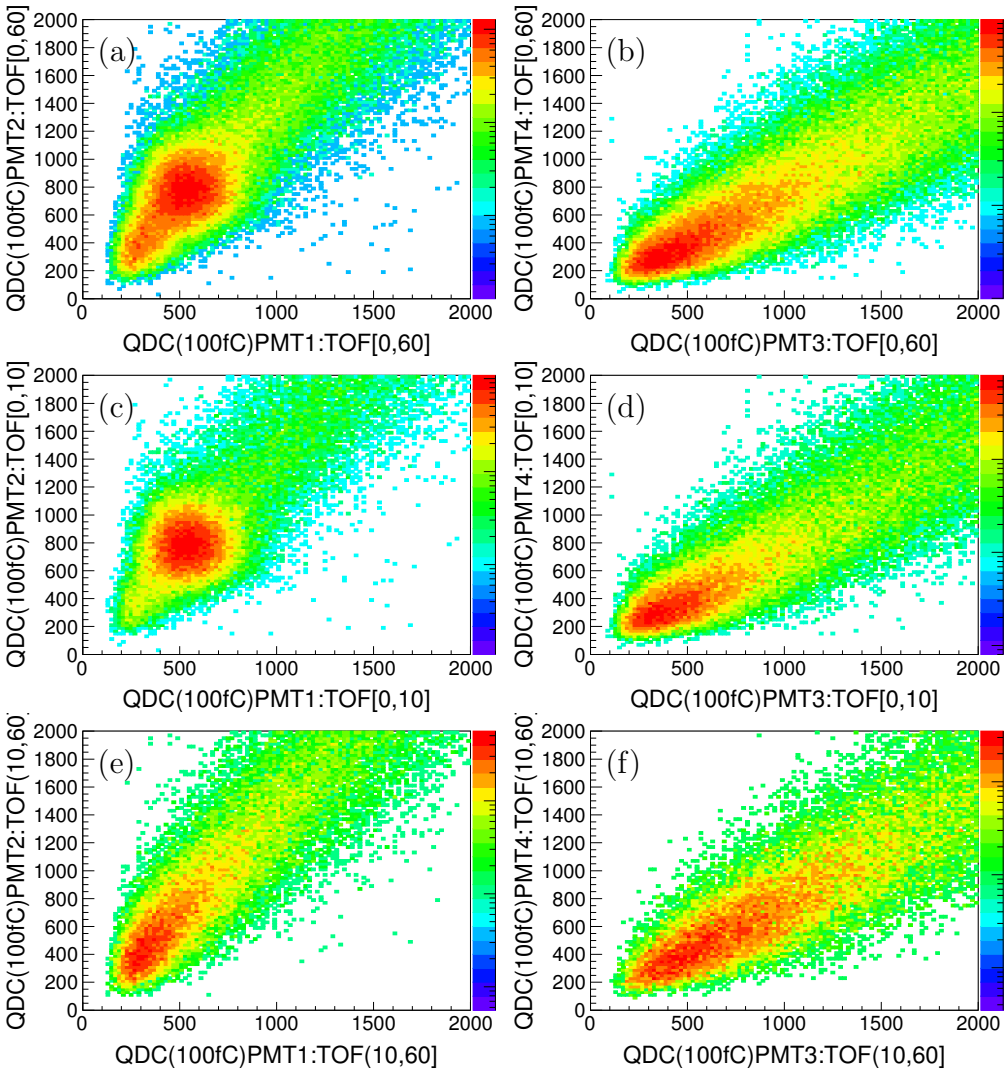

Figure 12: QDC correlation distribution within different TOF region from experiment setup2. (a) and (b) TOF region: [0, 60]. (c) and (d) TOF region: [0, 10]. (e) and (f) TOF region: [10, 60].

The fitting results are shown in the Figure 13, the number of thermal neutron is obtained to be 24162.0 ± 222.7. Background events are from the gamma emitted by neutron source(AmBe). The number of gamma is about 28562.1 ± 232.4.

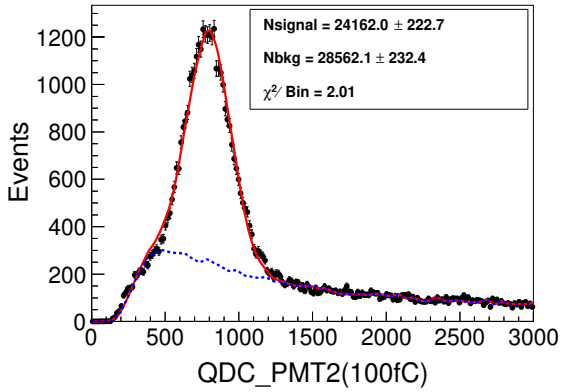

Figure 13: Fit result of QDC distribution measured by PMT2 from experiment setup2 and TOF region: [-20, 10].

4. Conclusion

In this article, we take advantage of characteristic gamma (480 keV) from thermal neutron capture reaction on ^{10}B and develop a new TOF method to identify fast neutron, thermal neutron and gamma. Although PSD method can be used for identifying neutron and gamma, it is difficult to distinguish fast neutron and thermal neutron [8]. The commercial EJ276 [6] meterial is a pulse-shape discriminating plastic scintillator. If combining PSD with TOF method that use EJ276 plastic scintillator to replace EJ200 [5] in our experiment, it will make up for the shortcomings of PSD method and identify them completely.

5. Acknowledgments

Thank Baochen Wang and Lian Chen for their help and maintaining $^{241}AmBe$ (α, n) neutron source. R & D of neutron detector is part of Accelerator Driven Sub-critical System (ADS). This work is supported by Strate-

gic Priority Research Programs (Category A) of the Chinese Academy of Sciences.

References

[1] Knoll Glenn F. Knoll. Radiation Detection and Measurement, third ed., Wiley, New York, 1999.

[2] F. Pino, Applied Radiation and Isotopes 92 (2014) 6C11.

[3] Tibor Jacob Hajagos, Nuclear Instruments and Methods in Physics Research A 825 (2016) 40C50.

[4] http://www.eljentechnology.com/index.php/products/plastic-scintillators/ej-254.

[5] http://www.eljentechnology.com/index.php/products/plastic-scintillators/ej-200-ej-204-ej-208-ej-212.

[6] http://www.eljentechnology.com/images/products/data_sheets/EJ-276.pdf.

[7] YanFeng Wang, ZhiJia Sun, SCIENCE CHINA ,October 2013 Vol.56 No.10: 1897C1902

[8] Nuclear Instruments and Methods in Physics Research A 751 (2014) 62C69.

[9] 123.